Optical Materials 80 (2018) 203–208

Contents lists available at ScienceDirect

Optical Materials

journal homepage: www.elsevier.com/locate/optmat

Photoluminescence inhomogeneity and excitons in CVD-grown monolayer WS_2

Dan-Dan Ren[a,b], Jing-Kai Qin[a,b], Yang Li[a,b], Peng Miao[c], Zhao-Yuan Sun[a], Ping Xu[c], Liang Zhen[a,b], Cheng-Yan Xu[a,b,*]

[a] MIIT Key Laboratory of Advanced Structural-Functional Integration Materials & Green Manufacturing Technology, School of Material Science and Engineering, Harbin Institute of Technology, Harbin, 150001, China
[b] MOE Key Laboratory of Micro-Systems and Micro-Structures Manufacturing, Harbin Institute of Technology, Harbin, 150080, China
[c] School of Chemistry and Chemical Engineering, Harbin Institute of Technology, Harbin, 150001, China

ARTICLE INFO

Keywords:
WS_2
Photoluminescence
Exciton
Chemical vapour deposition
Transition metal dichalcogenides

ABSTRACT

Transition metal dichalcogenides two-dimensional materials are of great importance for future electronic and optoelectronic applications. In this work, triangular WS_2 monolayers with size up to 130 μm were prepared via chemical vapor deposition method. WS_2 monolayers presented uniform Raman intensity, while quenched photoluminescence (PL) was observed in the center. The PL quenching in the central part of WS_2 monolayer flakes was attributed to the gradually increasing sulfur vacancies toward the center. The proportion of negative trion (X^-) in PL spectrum increases with increasing sulfur vacancies in WS_2. The enhanced binding energy of X^- suggests higher Fermi level and n-doping level with larger sulfur vacancy concentration. Our findings may be beneficial to the development of integrated devices, and also explore the defect-induced optical and electrical properties for nanophotonics.

1. Introduction

In pace with the exploration of graphene since 2004 [1], two-dimensional (2D) materials of transition metal dichalcogenides (TMDs), such as MoS_2, $MoSe_2$, WS_2 and WSe_2, have drawn great attention for their unique electronic and optical properties induced by the quantum confinement at the 2D limit. Different from multilayer counterpart, monolayer semiconducting TMDs present strong light-matter interaction and efficient valley polarization due to their tunable direct bandgap [2–4] and spin-valley coupling [5]. Monolayer tungsten disulfide (WS_2) is known for its high quantum yield and resultant photoluminescence [6,7], which endow it as promising material for optoelectronics and nanophotonics. For example, square roots relationship between photocurrent and the incident power [8] and high responsivity of 53.3 A/W [9] can be achieved in WS_2 monolayer films-based photosensors. It is also a robust platform to reveal the spin and valley physics due to the large spin-orbit coupling in monolayer WS_2 [10–12]. Giant spin-valley coupling in WS_2 suppresses the interlayer hopping at valence band edge, resulting in layer-independence of the splitting of hot luminescence peaks [10].

Monolayer WS_2 is a desirable material for next-generation electronics and optoelectronics. Mechanical exfoliation, a feasible method to thin down bulk TMD materials, is incapable to obtain large-area monolayers [13–15]. Chemical vapor deposition (CVD) is a reliable way to obtain high quality TMDs monolayers with large enough lateral sizes for device fabrication [16–19]. However, during the CVD growth process, the structural defects, i.e. sulfur vacancies and dislocations, inevitably exist in CVD-grown monolayers on inert substrates [20–22]. A rich variety of defects and dislocation cores were observed in CVD grown MoS_2, such as monosulfur vacancy, disulfur vacancy and vacancy complex [21]. Different types of vacancies have also been observed in CVD-grown WS_2 through high-resolution transmission electron microscopy (HRTEM) observation [22]. Such defects introduce deep states in the band gap [20], which will definitely affect the optical [23] and electrical [24] properties of TMDs.

High quantum yield and PL intensity of monolayer WS_2 have been identified by time-resolved photoluminescence (TR-PL) spectroscopy at room temperature [7]. Many intriguing PL features have been unrevealed in CVD-grown WS_2, and PL inhomogeneity in lateral dimension has been reported in previous work [6,25–27]. Enhanced PL emission at the edge of CVD-grown WS_2 domains was reported, which was thought to be caused by the dielectric environment, strain and

* Corresponding author. MIIT Key Laboratory of Advanced Structural-Functional Integration Materials & Green Manufacturing Technology, School of Material Science and Engineering, Harbin Institute of Technology, Harbin, 150001, China.
E-mail address: cy_xu@hit.edu.cn (C.-Y. Xu).

https://doi.org/10.1016/j.optmat.2018.04.043
Received 24 February 2018; Received in revised form 9 April 2018; Accepted 22 April 2018

structural defects [6,25]. The gradual decline of PL intensity from edge to center of WS_2 flakes was thought to be attributed to S vacancies [26]. The edge enhancement of PL in monolayer WS_2 was resulted from bi-exciton emission from edges according to previous experiments [27].

The excitonic states are important features of two-dimensional TMDs, as the optical properties of semiconductors are mainly determined by their excitonic behaviours. There are neutral excitons, positive/negative trions and biexcitons in TMDs, and their PL peak intensities response differently to light illumination. WS_2 is expected to be an ideal material to investigate the optical behaviours for its multiple types of excitonic states. Various kinds of excitonic states have been identified in exfoliated single-layer WS_2 by temperature-dependent photoluminescence, indicating that the neutral and charged excitions can both exist in monolayer WS_2 from low temperature (4 K) to room temperature [28]. The biexciton emission has been detected by power-dependent PL in CVD-grown bilayer WS_2 [29], suggesting the strong quantum confinement and high exciton density in CVD WS_2.

In this work, we prepared triangular WS_2 monolayers on SiO_2 surface via CVD method. The inhomogeneity of photoluminescence (PL) intensity across the lateral dimension of WS_2 monolayer induced by unevenly distributed defects was investigated. The high sulfur vacancy density in the center of WS_2 monolayers leads to change in excitonic states, which is a dominant contribution for the PL quenching. Recombination of negative trions plays a dominant role in PL than uncharged excitons in high sulfur vacancy density position (center), suggesting a higher charged carrier density in the center of CVD-grown WS_2 flakes based on the mass action law. And higher binding energy of trions in the center suggests that the increasing sulfur vacancy leads to a higher n-doping level. The study of excitonic behaviour of monolayer WS_2 offers an approach to understand the relationship between crystal quality of TMDs and their optical properties.

2. Experimental

2.1. CVD growth of WS_2

Chemical vapor growth of WS_2 monolayers were conducted in a quartz tube furnace with two heating zones. S powder (0.5–0.8 g, 99%, Sigma Aldrich) and WO_3 powder (0.2–0.3 g, 99.995%, Sigma Aldrich) served as precursors in the sulfurization of WO_3 process. Along the airstream, S powder was spread on a quartz plate at the low-temperature heating zone (200–250 °C), and then WO_3 powder and SiO_2/Si wafers were placed at the open end of a one-end sealed quartz tube at the center of high-temperature heating zone (800–900 °C). Considering the small amount of tungsten vapor due to the high melting point (1473 °C) of WO_3, the one-end sealed quartz tube served as a collector of tungsten to make sure enough tungsten reaches SiO_2 surface. The two zones were heated at a ramping rate of 20 °C/min to 200–250 °C and 800–900 °C, respectively, and the first zone was started later to make sure that the two zones reached deserved temperature at the same time. Argon gas (60 sccm) was introduced at the beginning of the heating procedure and 20 sccm mixed gas (75% Ar + 25% H_2) was introduced once it reaches the deserved temperature. After the growing of WS_2 layers, the whole furnace was cooling down naturally.

2.2. TEM sample preparation

WS_2 layers on SiO_2 surface were covered with a thin layer of polymethyl methacrylate (PMMA) by spin coating at 3000 rpm for 60 s. Next, the samples were treated at 60 °C for 2 h in a drying cabinet. Hydrofluoric acid solution (~20%) was used to dissolve SiO_2 layers, and PMMA films were lifted from the substrates. Finally, the PMMA film with WS_2 layers were transferred to carbon-supported Cu grids, and then acetone was used to remove PMMA to leave WS_2 layers on the grids. Transmission electron microscope (TEM) test was performed at FEI Tecnai G^2 F30 microscope.

2.3. Raman and PL measurements

Raman and PL measurements were performed on Renishaw inVia Raman microscope at λ_{ex} = 532 nm using a × 100 objective.

3. Results and discussion

The optical micrograph (OM) image in Fig. 1a shows that WS_2 flakes grown at 870 °C for 1 h on SiO_2 surface exhibit triangular shape, with lateral sizes ranging from 30 to 130 μm. The morphology evaluation within the distance between tungsten source and SiO_2 substrates is provided in Fig. S1, and other morphologies observed in our CVD attempts are shown in Fig. S2. The uniform contrast in OM indicates uniform thickness of WS_2 monolayers. Fig. 1b presents typical atomic force microscopy (AFM) image of a WS_2 monolayer with thickness of 0.9 nm. Transmission electron microscope was employed to investigate the structure of monolayer WS_2. High-resolution transmission electron microscopy (HRTEM) image (Fig. 1c) and selected-area electron diffraction (SAED) pattern (Fig. 1d) with [0001] zone axis confirm the expected hexagonal lattice structure with lattice spacings of 0.27 and 0.16 nm, corresponding to the lattice space spacing of $(2\bar{1}\bar{1}0)$ and $(11\bar{2}0)$ planes, respectively.

Raman spectroscopy is utilized to identify monolayer WS_2 and its crystal quality. Fig. 2 shows the Raman spectrum of monolayer WS_2 with light excitation of 532 nm. According to multi-Lorentzian fitting, the prominent combined peak at ~350 cm^{-1} contains three sub-peaks: in-plane vibration $E^1_{2g}(M)$ mode at 342 cm^{-1}, second-order mode of longitudinal acoustic phonon 2LA(M) mode at 350 cm^{-1} and in-plane vibration $E^1_{2g}(\Gamma)$ mode at 354 cm^{-1}. The out-of-plane vibration A_{1g} mode is located at 417 cm^{-1}, and the intensity ratio of $E^1_{2g}(\Gamma)/A_{1g}$ is about 2.1, suggesting the formation of perfect monolayer according to previous work [30]. The Raman signature is coincident with the *ab* initio calculations of the phonon dispersions of monolayer WS_2 [31]. Also, combination modes $2LA(M) - 2E^2_{2g}(\Gamma)$ and $2LA(M) - E^2_{2g}(\Gamma)$ are observed at 294 cm^{-1} and 321 cm^{-1}, respectively. Uniform Raman intensity ($E^1_{2g}(\Gamma)$) across individual monolayer WS_2 is presented in the

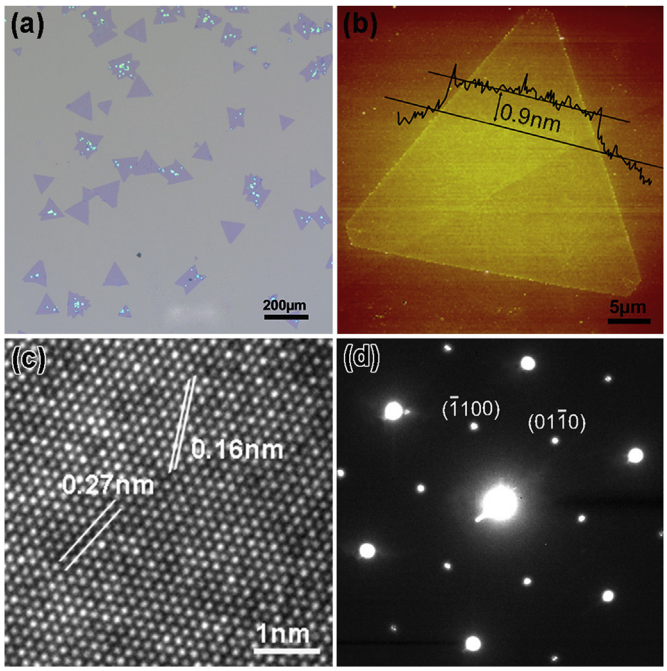

Fig. 1. (a) Optical micrograph of WS_2 monolayers grown at 870 °C; (b) AFM topography image and height profile of WS_2 monolayer; (c) HRTEM image of monolayer WS_2; (d) SAED pattern taken along [0001] zone axis.